

A Wavelet Approach for Estimating Chlorophyll-A From Inland Waters With Reflectance Spectroscopy

Eva M. Ampe, Erin L. Hestir, Mariano Bresciani, Elga Salvatore, Vittorio E. Brando, Arnold Dekker, Tim J. Malthus, Maarten Jansen, Ludwig Triest, and Okke Batelaan

Abstract—This letter presents an application of continuous wavelet analysis, providing a new semi-empirical approach to estimate Chlorophyll-a (Chl-a) in optically complex inland waters. Traditionally spectral narrow band ratios have been used to quantify key diagnostic features in the remote sensing signal to estimate concentrations of optically active water quality constituents. However, they cannot cope easily with shifts in reflectance features caused by multiple interactions between variable absorption and backscattering effects that typically occur in optically complex waters. We use continuous wavelet analysis to detect Chl-a features at various wavelengths and frequency scales. Using the wavelet decomposition, we build a 2-D correlation scalogram between *in situ* pond reflectance spectra and *in situ* Chl-a concentration. By isolating the most informative wavelet regions via thresholding, we could relate all five regions to known inherent optical properties. We select the optimal feature per region and compare them to three well-known narrow band ratio models. For this experimental application, the wavelet features outperform the NIR-red models, while fluorescence line height (FLH) yield comparable results. Because wavelets analyze the signal at different scales and synthesize information across bands, we hypothesize that the wavelet features are less sensitive to confounding factors, such as instrument noise, colored dissolved organic matter, and suspended matter.

Index Terms—Chlorophyll-a (chl-a), frequency analysis, high spectral resolution remote sensing, optically complex waters, wavelets.

I. INTRODUCTION

OPTICAL remote sensing has long been recognized as an effective solution for the assessment and monitoring of

Manuscript received October 10, 2012; revised January 4, 2013; accepted February 8, 2013. Date of publication March 13, 2013; date of current version November 8, 2013. This work was supported in part by the HOA-HYPERENV Project of the Vrije Universiteit Brussel, by CSIRO's Division of Land and Water, and Water for a Healthy Country Flagship, and by FWO project G.0949.10N.

E. M. Ampe and E. Salvatore are with the Department of Hydrology and Hydraulic Engineering, Vrije Universiteit Brussel, Brussels 1050, Belgium, and also with VITO, Flemish Institute for Technological Research, Mol 2400, Belgium (e-mail: eva.ampe@vub.ac.be).

E. L. Hestir, V. E. Brando, A. Dekker, and T. J. Malthus are with CSIRO, Land and Water, Canberra, ACT 2601, Australia.

M. Bresciani is with IREA-CNR, Milano 20133, Italy.

M. Jansen is with the Departments of Mathematics and Computer Science, Université Libre de Bruxelles, Brussels 1050, Belgium.

L. Triest is with the Department of Biology, Plant Science and Nature Management, Vrije Universiteit Brussel, Brussels 1050, Belgium.

O. Batelaan is with the Department of Hydrology and Hydraulic Engineering, Vrije Universiteit Brussel, Brussels 1050, Belgium, and also with the School of the Environment, Flinders University, Adelaide 2100, Australia.

Color versions of one or more of the figures in this paper are available online at <http://ieeexplore.ieee.org>.

Digital Object Identifier 10.1109/LGRS.2013.2247021

inland water quality. Due to the optical complexity of most inland water bodies, high spectral resolution data are needed to estimate concentrations of the optically active constituents in the water column [1], [2]. Chlorophyll-a (Chl-a, $\mu\text{g/l}$) concentration, a widely used water quality indicator of trophic status, is the most commonly estimated constituent from optical remote sensing [3]–[5]. Semi-empirical techniques are based on a statistical relationship between the water quality variable of interest and the remote sensing signals. Such approaches are usually easily implemented with existing *in situ* data, and often produce reliable results for the areas and data sets from which they are derived. Moreover, the spectral features used are often linked to the inherent optical properties of interest [4], [6], [7].

Semi-empirical algorithms for Chl-a estimation can be broadly classified into four categories: NIR-red-based narrow-band, fluorescence/reflectance line height, broad-band, and advanced such as neural networks and genetic algorithms. A detailed description of these algorithms can be found in review papers [4], [7] and references therein. With the exception of some sophisticated approaches [1], [8] that find the optimal band positions iteratively, current semi-empirical techniques use only a fraction of the available spectral information because they are fixed to certain wavelengths. This is especially problematic in optically complex waters where the optically active constituents may vary independently, Chl-a feature detection may be impeded by the influence of other optically active constituents [e.g., suspended matter and colored dissolved organic matter (CDOM)], and Chl-a spectral absorption features vary in both depth and width [9], [10]. Therefore, for optically complex waters, algorithms are needed that take full advantage of spectrally contiguous information across varying scales and are flexible in their feature detection.

Wavelets provide a potential solution for improved Chl-a feature detection from high spectral resolution data. They can be used to analyze the remote sensing signal at varying feature frequency scales as they extract spectral features at various wavelet scales. Scale is the characteristic width of a feature in a signal. It is the inverse of the rate or frequency at which the feature occurs. Fine wavelet scales extract narrow, high frequency features, and coarser wavelet scales describe broader low frequency features [10], [11]. In wavelength space subtle Chl-a features may be hidden by high frequency noise. However, in multiscale wavelet space Chl-a features may occur as features in coarser wavelet scales. Conversely, the finest

wavelet scales can capture the high frequency components of the signal, which are often noise [12].

Wavelets have been used in combination with high spectral resolution data in terrestrial remote sensing to capture features of different wavelet scales and positions in diverse applications, e.g., 1) building spectral libraries for spectral mixture analysis as wavelets decompose the spectrum into linearly additive wavelets that isolate spectral features from their continuum [10]; and 2) establishing relationships between the wavelet coefficients, derived from the remote sensing signal and an independent variable (e.g., to detect leaf chlorophyll concentration [13], to detect green attack damage due to mountain pine beetles [12], or leaf water content [11]).

This letter applies continuous wavelet analysis [12], providing a new semi-empirical approach to estimate Chl-a from high spectral resolution reflectance measurements in optically complex inland waters. Section II presents the continuous wavelet transform. Section III describes the experimental application and data acquisition. Section IV describes the results and discussion, and we conclude in Section V.

II. CONTINUOUS WAVELET TRANSFORM

We used the continuous wavelet transform, which is well suited to analyze high spectral resolution data at arbitrary frequency scales [10], [12], [14]. Moreover, the output is readily comparable to the original wavebands, which benefits its interpretability [10]–[12]. Henceforth, the term wavelet will refer to the continuous wavelet transform. All analyses were performed using the *wmts* package in R version 2.15.1 [15].

The wavelet $\psi_{a,b}(\lambda)$ ($\lambda = 1, 2, \dots, n$, with n the number of wavebands) itself is constructed by shifting and scaling a mother wavelet $\psi(\lambda)$. The mother wavelet is shifted over different wavebands, and scaled by stretching the mother wavelet when it moves from a fine wavelet scale to a coarser wavelet scale by

$$\psi_{a,b}(\lambda) = \frac{1}{\sqrt{a}} \psi\left(\frac{\lambda - b}{a}\right) \quad (1)$$

where a and b represent the scaling and shifting factor, respectively, being both positive real numbers [11]. Based on both the shape of the remote sensing signal and its absorption features [11], we chose the Mexican hat (i.e., second derivative of Gaussian) as the mother wavelet [16]. The wavelet coefficients measure the correlation between a particular wavelet (for a particular wavelet scale and waveband) and the remote sensing signal at that waveband location [11]. They are calculated by convolving a wavelet with the remote sensing signal by

$$W_f(a, b) = \langle f, \psi_{a,b} \rangle = \int_{-\infty}^{+\infty} f(\lambda) \psi_{a,b}(\lambda) d\lambda \quad (2)$$

where $f(\lambda)$ is the remote sensing signal and $W_f(a, b)$ are the resulting wavelet coefficients forming a 2-D matrix for the different wavelengths and wavelet scales [11]. Per scale, we computed a 95% support interval $[b - I, b + I]$, satisfying

$$\int_{b-I}^{b+I} \psi_{a,b}^2(\lambda) d\lambda = 0.95. \quad (3)$$

III. EXPERIMENTAL APPLICATION

A. Study Site

We investigated 21 artificial shallow ponds (depth <3 m) located in the Brussels Capital Region, Belgium. The ponds were created by damming of low-order streams in the 20th century or earlier. They are flat-bottomed with a surface area ranging from 0.1 to 6.0 ha. They were selected because they are easy to reach and show a range of water quality characteristics, while having the same climate and hydrology, creating an optimal setting for an experimental application. The ponds are affected by eutrophication caused by historical and current urban pollution in varying degrees [17]. Water quality measurements were collected in support of the BBlooms 2 project (Belgian Science Policy) [17]. The project aimed at monitoring, identifying, and predicting cyanobacterial and algal blooms. In August 2009 and July 2010, the project collected integrated water column samples from ten random subsamples spatially distributed across each pond using a plastic tube sampler. From the pooled sample they measured chemical variables and Chl-a (1.6–478.3 $\mu\text{g/l}$) according to [17]. Algae counts using inverted microscope confirmed the presence of cyanobacteria in nine ponds.

B. High Spectral Resolution Data

In order to provide the best possible match-up between the *in situ* spectral measurements and the integrated Chl-a measurements from Section III-A [17], we computed pond-level percent reflectance ($R(\lambda)$, Fig. 1) based on spectral measurements collected within 24 h of the water quality sampling. $R(\lambda)$ was computed as

$$R(\lambda) = \left(\frac{\text{Upwelling above water radiance}}{\text{Downwelling radiance}} \right) \cdot 100. \quad (4)$$

To obtain $R(\lambda)$, we collected more than 25 above water radiance measurements during solar noon from nadir at two different locations per pond. We measured: 1) the upwelling above water radiance approximately 1.5 m above the water surface, and 2) the downwelling radiance from a Spectralon panel. We used a Ramses-ARC radiance sensor (TriOs, Oldenburg, Germany), which has a field of view of 7deg, a wavelength range of 320–950 nm, 190 usable bands and a resolution (Rayleigh-criterion) of 10 nm [18].

C. Correlation Scalogram and Feature Selection

Each wavelet scale can be considered a different representation of the $R(\lambda)$; thus, the wavelet coefficients can be used as estimators in a regression model. Here, the coefficients are used to estimate Chl-a from $R(\lambda)$. In order to simultaneously assess narrow and broad Chl-a reflectance features, we produced a 2-D correlation scalogram, showing where in wavelength space the Chl-a features are located, and at which wavelet scale. This methodology is adapted from [12]; however, we do not assume the data to be normally distributed.

We performed the following steps.

- 1) We calculated wavelet coefficients for each $R(\lambda)$, resulting in 21 2-D wavelet coefficient matrices.

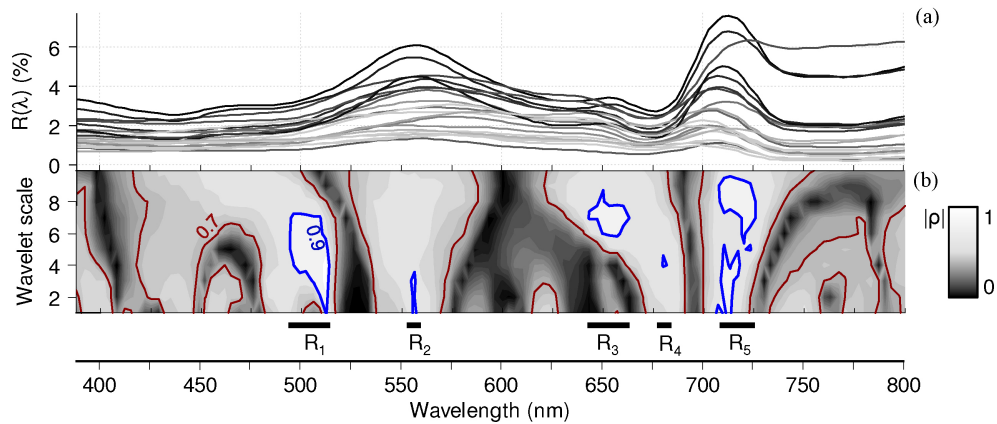


Fig. 1. (a) Pond-level percent reflectance ($R(\lambda)$). The gray scale is related to the corresponding *in situ* Chl-a concentration (1.6–478.3 $\mu\text{g/l}$), light gray indicating low concentrations through black indicating high concentration. (b) Wavelet correlation scalogram. Isolines indicate where $|\rho|$ is equal to 0.70 (red) and 0.90 (blue). The informative wavelet regions (R_1 – R_5) where $|\rho| > 0.9$ are displayed below the scalogram.

- 2) We calculated the absolute value of the Spearman correlation coefficient $|\rho|$ between the wavelet coefficients and the Chl-a concentration at each pond. The $|\rho|$ is calculated for each wavelength and wavelet scale.
- 3) We built a 2-D correlation scalogram displaying the calculated $|\rho|$ for all the wavelengths and wavelet scales.
- 4) We selected the informative wavelet regions (R_1 , R_2 , \dots , R_k , with k representing the number of regions) by thresholding $|\rho|$ at 0.90. For each region, we selected the wavelength and wavelet scale that has the highest $|\rho|$ as the most informative wavelet feature (F_1 , F_2 , \dots , F_k).
- 5) We investigated the relationship between the Chl-a and the informative wavelet features. Based on this analysis, we selected an exponential regression model. The regression models were assessed using the R^2 , root mean square error (RMSE), the second-order Akaike information criterion (AICc), and Bayesian information criterion (BIC) [21].

D. Narrow Band Models

We compared the results of the wavelet regression models to three narrow band models (Table I) calculated on $R(\lambda)$: 1) a two-band NIR-red model; 2) a three-band NIR-red model; and 3) the fluorescence line height algorithm (FLH). NIR-red, two- or three-band, algorithms are among the most popular semi-empirical approaches for estimating Chl-a concentration in optically complex waters [4], [19]. They are based on the optical information in the NIR-red region. This spectral region is useful for estimating Chl-a in optically complex waters, as it is less influenced by variations in the spectral properties of suspended matter and CDOM [7], [19]. The FLH [20] is based on the fluorescence emission band at 681 nm. The FLH is a linear baseline algorithm for $<30 \mu\text{g/l}$ Chl-a ranges [4], [7], [22]. For each model, we selected the regression model with the best fit for Chl-a prediction: linear for the NIR-red models and exponential for the FLH and wavelet models. We evaluated the model performance as described in Section III-C.

IV. RESULTS AND DISCUSSION

A. Distinguishing Informative Wavelet Regions

The application of wavelets to the high spectral resolution data resulted in detection of broad and narrow Chl-a

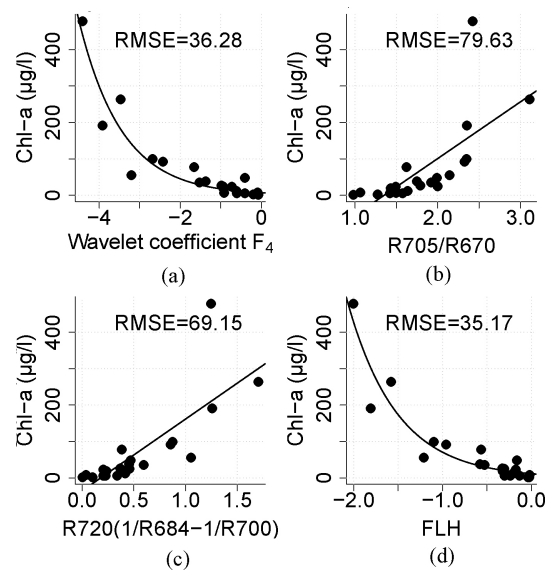


Fig. 2. Chl-a estimates by (a) wavelet feature 4 (F_4), (b) two-band model, (c) three-band model, and (d) FLH model. For each diagnostic feature (wavelet or narrow band model), we fit the regression model with the best fit (linear or exponential) for Chl-a prediction.

reflectance features. A high correlation coefficient in the correlation scalogram [Fig. 1(b)] at the fine wavelet scales [low scales, Fig. 1(b)] indicates that the convolution of the Mexican hat wavelet in a narrow window around the center waveband correlates well with the Chl-a concentration. Analogously, at coarse wavelet scales (high scales), a larger window around the center waveband correlated well with the Chl-a concentration. We identified five informative wavelet regions (R_1 – R_5), two were located in the blue–green region, and three were located in the red-NIR region [Fig. 1(b)].

R_1 is centered at 512 nm on the left shoulder of the reflectance peak at 550 nm. It starts narrow at wavelet scales one and two and becomes wider at wavelet scales three through seven. It is part of one large region where $|\rho| > 0.70$ throughout all the wavelet scales, indicating that R_1 is part of a prominent spectral feature in $R(\lambda)$. The same is true for R_2 , which is narrow and present at wavelet scales one through three. It is located on the first reflectance peak in the blue-green region.

TABLE I
TWO-, THREE-BAND, AND FLH MODEL USED TO ESTIMATE CHL-A

Model Name	Formula	Citation
Two-band	$\frac{R705}{R670}$	Gitelson <i>et al.</i> [19]
Three-band	$R720 \left(\frac{1}{R684} - \frac{1}{R700} \right)$	Gitelson <i>et al.</i> [8]
FLH	$R682 - R665 - \frac{(R705 - R665)(682 - 665)}{(705 - 665)}$	Gower <i>et al.</i> [20]

TABLE II
CENTER WAVELENGTH, WAVELET SCALE, AND 95% SUPPORT INTERVAL OF THE FIVE INFORMATIVE WAVELET FEATURES (F₁-F₅)

	F ₁	F ₂	F ₃	F ₄	F ₅
Center wavelength	512 nm	556 nm	657 nm	680 nm	723 nm
Wavelet scale	4	1	7	4	8
95% support	482–534 nm	549–563 nm	603–710 nm	650–710 nm	663–783 nm

This peak is known as a diagnostic of minimal absorption caused by algal pigments coupled with scattering by phytoplankton cell walls and non-organic suspended matter [19]. Indeed, R₁ and R₂ correspond to MERIS, Oceansat-1 OCM and SeaWiFS bands four and five and R₂ to MODIS band four, which are often used as a ratio in ocean optics to detect Chl-a [7], [20], [23]. Application of these blue green wavelengths in eutrophic and optically complex waters is however limited for estimating Chl-a [7], as scattering and absorption from suspended matter and CDOM are superimposed on the signal [19], [24]. This superposition may also be the reason for the absence of an informative wavelet region around the maximum Chl-a absorption at 440 nm [2], [19].

Another wide region ($|\rho| > 0.7$) occurs across wavelength 625–680 nm at high wavelet scales (8–10) and narrows to 670–690 nm at fine wavelet scales (1–4). It contains two informative wavelet regions ($|\rho| > 0.9$), R₃ and R₄. R₃ is located around the shoulder of a large reflectance peak, and is only present at intermediate wavelet scales (6–8). It is influenced at shorter wavelengths by absorption in the range of 620–630 nm by phycocyanin a pigment present in cyanobacteria [19], [25] and at longer wavelengths by the second Chl-a absorption maximum around 670 nm [2], [19]. R₄, is only present at one wavelength and wavelet scale, indicating a subtle reflectance feature. Resting to the left of the second Chl-a absorption reflectance feature at 670 nm, R₄ is likely diagnostic of both this Chl-a absorption and the second reflectance peak around 710 nm, which is related to a combined reflectance minimum due to Chl-a and water absorption coupled with high reflectance due to scattering from all suspended matter including phytoplankton biomass [19]. In addition, R₄ is colocated with the fluorescence emission band. Visually, the fluorescence peak could not easily be detected as it can be masked or shifted due to absorption due to water and Chl-a [4], [22]. It is, therefore, possible that R₄ detected the subtle frequency of the fluorescence emission band. However, because the wavelet filter works over several wavelengths, it also incorporates information of the neighbouring Chl-a features.

R₅ stretches from wavelet scale one through nine, indicating that it is related to a prominent reflectance feature in the $R(\lambda)$. It starts near the reflectance peak around 710 nm at fine wavelet scales and rests on the NIR shoulder of this peak at higher wavelet scales where it widens and stretches over five

TABLE III
RESULTS OF THE EXPONENTIAL REGRESSION FOR THE WAVELET FEATURES AND FLH, AND THE LINEAR REGRESSION FOR THE TWO- AND THREE-BAND MODEL

Feature	R ²	RMSE	AICc	BIC	Model (Chl-a=)
F ₁	0.88	38.09	219.14	221.61	$14.22 \cdot e^{-3.37 \cdot F_k}$
F ₂	0.85	42.53	223.78	226.24	$18.64 \cdot e^{25.20 \cdot F_k}$
F ₃	0.84	47.46	228.37	230.84	NS
F ₄	0.90	36.28	217.10	219.56	$6.84 \cdot e^{-0.94 \cdot F_k}$
F ₅	0.88	39.46	220.62	223.09	$14.81 \cdot e^{0.44 \cdot F_k}$
FLH	0.90	35.17	215.79	218.25	$11.69 \cdot e^{-1.80 \cdot F_k}$
2 band	0.49	79.63	250.11	252.58	$155.72 \cdot F_k - 210.46$
3 band	0.61	69.15	244.18	246.65	NS

NS: nonsignificant coefficients at $\alpha = 0.05$.

wavelengths, relating both shape and shift [2], [26] of this peak to Chl-a.

B. Informative Wavelet Features to Estimate Chl-a

We selected the optimal wavelet features (F₁–F₅) within the informative wavelet regions (R₁–R₅). The features center wavelength, wavelet scale, and 95% support interval (3) are listed in Table II. The 95% support interval indicates where 95% of the filter support is located in wavelength space. The wavelet scale influences the width of the wavelet. Larger wavelet scales include information from more wavebands, identifying broad features, while smaller wavelet scales highlight narrow features.

C. How Wavelets Compare to Narrow Band Models

The evaluation statistics are similar for the five wavelet features (Table III). However, we only display the scatterplot of F₄, as it resulted in the highest R² and the lowest RMSE, AICc, and BIC (Fig. 2 and Table III). F₃, on the other hand, exhibits the lowest R² and the highest RMSE, AICc, and BIC.

We use the RMSE (Fig. 2) to compare the exponential models of the wavelet features and the FLH to the linear regression models built on the NIR-red models (two- and three-band model). All five informative wavelet features (F₁–F₅) better predict the Chl-a concentration, compared to the NIR-red models as they exhibit a lower RMSE than the NIR-red models (Table III). The three-band model outperforms the two-band model (Fig. 2). The FLH model is comparable to wavelet

F₄. Whether the FLH is significantly better is undetermined; the RMSE, AICc, and BIC are lower, but the R² is equal. Both models use bands in the same wavelength region.

V. CONCLUSION

The presented results illustrated the potential of wavelet analysis of high spectral resolution data to estimate the Chl-a concentration in optically complex inland waters. Five informative wavelet regions were identified and could be related to the inherent optical properties of interest. The FLH model and the optimal wavelet feature performed comparably, most likely because they relied on the same wavelength region. For this experimental application of wavelets for Chl-a prediction, the wavelet method outperformed the NIR-red models because wavelets synthesize information over various bands in one coefficient over various frequency scales. In essence, both wavelets and narrow band models were used to capture the changes in spectral reflectance that indicated key diagnostic features of the remote sensing signal. Two of the five informative wavelet regions were colocated with these reflectance shoulders, keying in on the slope of absorption and reflectance features. However, by analyzing the remote sensing signal in frequency space across multiple scales, wavelets captured more information critical to Chl-a prediction than a ratio approach could. We hypothesized that because wavelets can analyze the signal at different scales and synthesize information across wavebands, the wavelet features were less sensitive to the confounding factors present in this letter, such as instrument measurement noise, and the likely but unquantified high concentrations of CDOM and suspended matter. Such confounding factors are likely to be present in many inland water quality applications, thus the wavelet approach may provide a suitable empirical approach for future studies. This study was a first experimental application of the continuous wavelet transform for Chl-a detection in inland water. Future research is needed to test the robustness of this method on an independent dataset.

ACKNOWLEDGMENT

The authors would like to thank T. Cheng, S. Delalieux, K. Hestir, D. Raymaekers, H. Sahli and B. Somers for the helpful discussions and insights, and the two anonymous reviewers for their useful comments and suggestions.

REFERENCES

- [1] W. J. Moses, A. A. Gitelson, R. L. Perk, D. Gurlin, D. C. Rundquist, B. C. Leavitt, T. M. Barrow, and P. Brakhage, "Estimation of chlorophyll-a concentration in turbid productive waters using airborne hyperspectral data," *Water Res.*, vol. 46, no. 4, pp. 993–1004, 2012.
- [2] H. J. Hoogenboom, A. G. Dekker, and I. A. Althuis, "Simulation of aviris sensitivity for detecting chlorophyll over coastal and inland waters," *Rem. Sens. Environ.*, vol. 65, no. 3, pp. 333–340, 1998.
- [3] M. Bresciani, D. Stroppiana, D. Odermatt, G. Morabito, and C. Giardino, "Assessing remotely sensed chlorophyll-a for the implementation of the water framework directive in european perialpine lakes," *Sci. Total Environment*, vol. 409, no. 17, pp. 3083–3091, 2011.
- [4] M. W. Matthews, "A current review of empirical procedures of remote sensing in inland and near-coastal transitional waters," *Int. J. Remote Sens.*, vol. 32, no. 21, pp. 6855–6899, 2011.
- [5] C. Giardino, V. E. Brando, A. Dekker, N. Strombeck, and G. Candiani, "Assessment of water quality in lake garda (Italy) using hyperion," *Rem. Sens. Environ.*, vol. 109, no. 2, pp. 183–195, 2007.
- [6] A. Cunningham, I. D. Carrie, and R. E. Korb, "Two-component modeling of the optical properties of a diatom bloom in the southern ocean," *Rem. Sens. Environ.*, vol. 115, no. 6, pp. 1434–1442, 2011.
- [7] D. Odermatt, A. Gitelson, V. E. Brando, and M. Schaepman, "Review of constituent retrieval in optically deep and complex waters from satellite imagery," *Rem. Sens. Environ.*, vol. 118, pp. 116–126, Mar. 2012.
- [8] A. A. Gitelson, B. C. Gao, R. R. Li, S. Berdnikov, and V. Saprygin, "Estimation of chlorophyll-a concentration in productive turbid waters using a hyperspectral imager for the coastal ocean: The Azov sea case study," *Environmental Res. Lett.*, vol. 6, no. 024023, p. 6, 2011.
- [9] V. E. Brando, A. G. Dekker, Y. J. Park, and T. Schroeder, "Adaptive semianalytical inversion of ocean color radiometry in optically complex waters," *Appl. Opt.*, vol. 51, no. 15, pp. 2808–2833, 2012.
- [10] B. Rivard, J. Feng, A. Gallie, and A. Sanchez-Azofeifa, "Continuous wavelets for the improved use of spectral libraries and hyperspectral data," *Rem. Sens. Environ.*, vol. 112, no. 6, pp. 2850–2862, 2008.
- [11] T. Cheng, B. Rivard, and G. A. Sánchez-Azofeifa, "Spectroscopic determination of leaf water content using continuous wavelet analysis," *Rem. Sens. Environ.*, vol. 115, no. 2, pp. 659–670, 2011.
- [12] T. Cheng, B. Rivard, G. A. Sánchez-Azofeifa, J. Feng, and M. Calvo-Polanco, "Continuous wavelet analysis for the detection of green attack damage due to mountain pine beetle infestation," *Rem. Sens. Environ.*, vol. 114, no. 4, pp. 899–910, 2010.
- [13] G. Blackburn and J. Ferwerda, "Retrieval of chlorophyll concentration from leaf reflectance spectra using wavelet analysis," *Rem. Sens. Environ.*, vol. 112, no. 4, pp. 1614–1632, 2008.
- [14] M. Jansen, "Multiscale change point analysis in poisson count data," *Chemometrics Intell. Lab. Syst.*, vol. 85, no. 2, pp. 159–169, 2007.
- [15] W. Constantine and D. Percival. (2011). *WMTSA: Wavelet Methods for Time Series Analysis*, r package version 1.1-1 [Online]. Available: <http://CRAN.R-project.org/package=wmtsa>
- [16] S. Muraki, "Multiscale volume representation by a dog wavelet," *IEEE Trans. Visualization Comput. Graph.*, vol. 1, no. 2, pp. 109–116, 1995.
- [17] S. Teissier, A. Peretyatko, S. De Backer, and L. Triest, "Strength of phytoplankton-nutrient relationship: evidence from 13 biomanipulated ponds," *Hydrobiologia*, vol. 689, no. 1, pp. 147–159, 2012.
- [18] Trios-Ramses. (2012, Jul.). *Ramses-Arc—Hyperspectral UV-VIS Radiance Sensor* [Online]. Available: <http://www.trios.de/>
- [19] A. A. Gitelson, Y. Z. Yacobi, J. F. Schalles, D. C. Rundquist, R. Han, L. Stark, and D. Etzion, "Remote estimation of phytoplankton density in productive waters," *Arch. Hydrobiol. Spec. Issues Advanc. Limnol.*, vol. 55, pp. 121–136, Feb. 2000.
- [20] J. F. R. Gower, R. Doerffer, and G. A. Borstad, "Interpretation of the 685 nm peak in water-leaving radiance spectra in terms of fluorescence, absorption and scattering, and its observation by meris," *Int. J. Remote Sens.*, vol. 20, no. 9, pp. 1771–1786, 1999.
- [21] C. M. Hurvich and C.-L. Tsai, "Regression and time series model selection in small samples," *Biometrika*, vol. 76, no. 2, pp. 297–307, 1989.
- [22] J. Gower, S. King, G. Borstad, and L. Brown, "Detection of intense plankton blooms using the 709 nm band of the meris imaging spectrometer," *Int. J. Remote Sens.*, vol. 26, no. 9, pp. 2005–2012, 2005.
- [23] P. Dash, N. D. Walker, D. R. Mishra, C. Hu, J. L. Pinckney, and E. J. D'Sa, "Estimation of cyanobacterial pigments in a freshwater lake using OCM satellite data," *Rem. Sens. Environ.*, vol. 115, no. 12, pp. 3409–3423, 2011.
- [24] G. Motwani, P. Chauhan, N. Sanwlani, and H. Solanki, "Optical characterization of backscattering by total suspended matter and its correlation with phytoplankton concentration in the Arabian Sea," in *Earth System Processes and Disaster Management* (Society of Earth Scientists Series, vol. 1). Berlin/Heidelberg, Germany: Springer, 2013, pp. 231–239.
- [25] H. J. Gons, H. Hakvoort, S. W. M. Peters, and S. S. G. H., *Harmful Cyanobacteria* (Aguatic Ecology Series, vol. 3), J. Huisman, M. H. C. P., and P. M. Visser, Eds. Dordrecht, The Netherlands: Springer, 2005.
- [26] A. Dekker, "Detection of optical water quality parameters for eutrophic waters by high resolution remote sensing," Ph.D. dissertation, Vrije Univ. Amsterdam, Amsterdam, The Netherlands, 1993.